Journal of Mineralogical and Petrological Sciences (2026) 121:012

Fe^{2+}-rich ferro-holmquistite from Japan: structural implications for the holmquistite group

Daisuke NISHIO-HAMANE[*], Mariko NAGASHIMA[**], Yuki MORI[***], Masayuki OHNISHI[†], Seiji HARADA[‡] and Etsuo HASHIMOTO[§]

[*]*Institute for Solid State Physics, the University of Tokyo, Kashiwa 277-8581, Japan*
[**]*Division of Earth Science, Graduate School of Science and Technology for Innovation, Yamaguchi University, Yamaguchi 753-8512, Japan*
[***]*Department of Life Science, Graduate School of Science, University of Hyogo, Himeji 671-2280, Japan*
[†]*Takehana Ougi-cho, Yamashina-ku, Kyoto 607-8082, Japan*
[‡]*Nanatsuike machi, Koriyama, Fukushima 963-8831, Japan*
[§]*Ipponmatsu, Hideyama, Asaka-machi, Koriyama, Fukushima 963-0101, Japan*

Ferro-holmquistite with high Fe^{2+} content, which was previously predicted to be unlikely to occur, has been identified from a dyke composed of quartz and microcline in limestone at Mt. Hayamadake, Tamura City, Fukushima Prefecture, Japan. The specimen was collected in the 1980s and had been preserved in a private collection as an unnamed amphibole species; however, its name and features have now been revealed as ferro-holmquistite. The empirical formula, estimated on the basis of the constraints of Si = 8 is $(\square_{0.93}Na_{0.07})_{\Sigma1}(Li_{1.97}Mg_{0.03})_{\Sigma2}(Fe^{2+}_{2.62}Mg_{0.20}Mn_{0.18}Al_{1.75}Fe^{3+}_{0.25})_{\Sigma5}Si_8O_{22.05}(OH_{1.96}F_{0.04})_{\Sigma2}$ for the platy-crystal sample. The unit-cell parameters obtained from single-crystal X-ray diffraction measurements are a = 18.4080(3) Å, b = 17.7942(3) Å, c = 5.29463(11) Å, and V = 1734.29(6) Å^3, with placement in the orthorhombic *Pnma* space group. Comparison of the single-crystal X-ray diffraction results with those for the holmquistite group reveals that the $M1$ and $M3$ octahedra expand with increasing Fe^{2+} content. In particular, the $M3$ octahedron exhibits marked distortion and anisotropic elongation, most notably along the ***b***-axis. Conversely, an increase in the Fe^{3+} content enlarges and distorts the $M2$ octahedron, while mitigating deformation at the $M1$ and $M3$ sites. The tetrahedral chain demonstrates structural flexibility in response to these changes, either by adjustment of the tetrahedral volume and/or alteration in the degree of chain kinking. Through these changes, the low bond valence sums for O4A and O4B, which were once considered the starting point of structural limitation, remain consistently low. As a result, the previously held notion that geometric constraints inhibit the formation of Fe^{2+}- and/or Fe^{3+}-rich members should be reconsidered.

Keywords: Ferro-holmquistite, Holmquistite, Ferro-ferri-holmquistite, Amphibole, Mt. Hayamadake

INTRODUCTION

Holmquistite, with the ideal formula of $\square Li_2(Mg_3Al_2)Si_8O_{22}(OH)_2$, is an amphibole characterized by a crystal structure that belongs to the orthorhombic *Pnma* space group. According to Cámara and Oberti (2005), holmquistite exhibits a crystal-chemical constraint that restricts the incorporation of cations larger than Mg and Al. The occurrence of ferro-holmquistite, defined by Fe^{2+} > Mg, has remained extremely rare, and even in such cases, the degree to which Fe^{2+} exceeds Mg has been minimal. However, ferro-ferri-holmquistite, in which Fe^{2+} > Mg and Fe^{3+} > Al, has more recently been established as a new mineral (Nagashima et al., 2022). This composition was

doi:10.2465/jmps.251128b
D. Nishio-Hamane, hamane@issp.u-tokyo.ac.jp Corresponding author

unexpected, given the assumption that the Fe^{2+} content would decrease as Fe^{3+} became more dominant in the holmquistite group. In addition to ferro-ferri-holmquistite, this study reports the occurrence of ferro-holmquistite with an equally unexpected composition, where Fe^{2+} far exceeds Mg, which results in a formula that approaches the ideal composition $\square Li_2(Fe^{2+}_3Al_2)Si_8O_{22}(OH)_2$ for ferro-holmquistite.

The occurrence of Fe^{2+}-enriched ferro-holmquistite is significant because it enables a clear distinction between the effects of Fe^{2+} and Fe^{3+}. Therefore, the description of ferro-holmquistite in the present investigation is expected to contribute to a deeper understanding of the crystal chemistry of the holmquistite group.

OCCURRENCE AND APPEARANCE

The Abukuma Plateau, located in eastern Fukushima Prefecture, Japan, is mainly composed of Cretaceous granitic rocks (e.g., Kubo et al., 2003). In the central part of the plateau, within the Tamura City area, limestone, shale, chert, and mafic rocks occur as xenoliths or roof pendants within the granitic rocks, distributed over an area approximately 10 km in the north-south direction and 5 km in the east-west direction. These rock bodies were collectively named the Takine Group by Ehiro et al. (1989). However, because neither fossils nor stratigraphic units that can be correlated with those in surrounding regions have been identified, the age of the Takine Group remains undetermined.

Ferro-holmquistite was found at Mt. Hayamadake in Tamura City, Fukushima Prefecture, Japan (37°25′30″N 140°38′21″E), where limestone is distributed as a roof pendant and pegmatites are known to occur (Omori and Hasegawa, 1957). The samples, including ferro-holmquistite, were collected by the authors (E. H. and S. H.) in the 1980s, and stored as amphibole specimens without a specific name for many years. Limestone is intruded by dykes composed mainly of quartz and microcline (Fig. 1a). The dyke had reacted with the surrounding limestone, and minerals such as axinite-(Fe), hedenbergite, spessartine, hellandite-(Y), pyrochlore-group minerals, löllingite, and fluorapatite had formed at the contact zone as fine particles within the dykes. Bornite and chalcopyrite were formed on the limestone side, and irregularly shaped grains of hessite, wittichenite, and parkerite ranging from a few micrometers to several tens of micrometers in size were observed within the bornite.

Ferro-holmquistite occurs as one of the constituent minerals of the dykes and is particularly abundant in their center (Fig. 1a). This occurrence suggests that most ferro-holmquistite was formed at the latest stage of the solidification of dyke. It is noted that the occurrence of tourmaline has not been confirmed in either the dykes or the limestone. The formation of axinite-(Fe) and hellandite-(Y) may have consumed boron, which prevents the formation of tourmaline, and could otherwise play a role as a host for lithium. In this dyke, the only host mineral for Li was ferro-holmquistite.

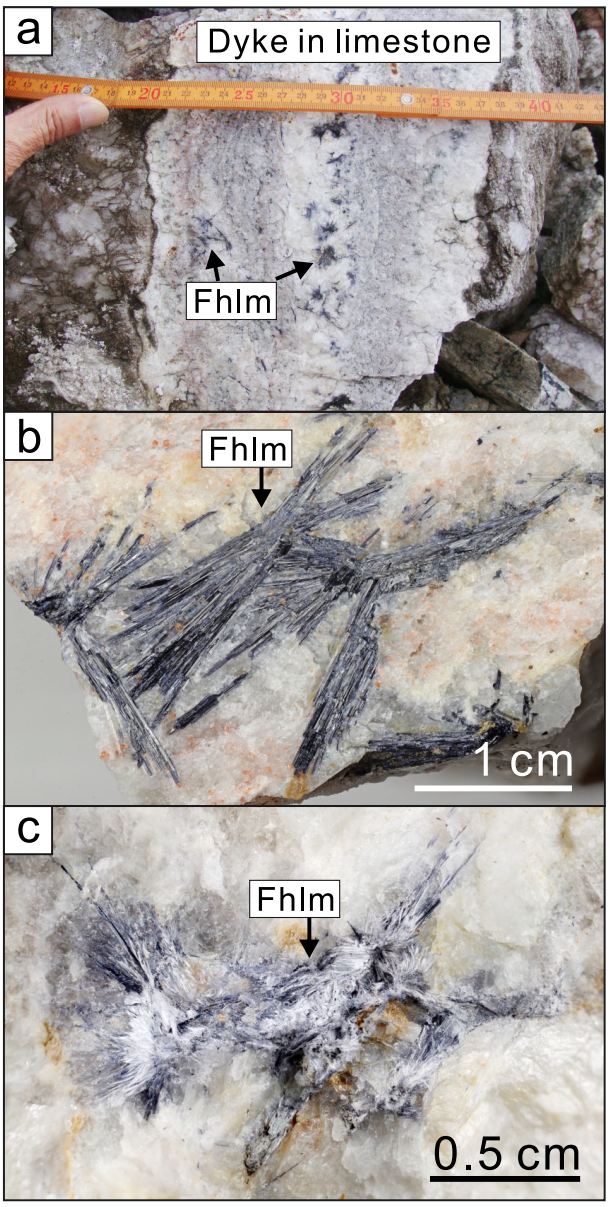

Figure 1. Occurrence of ferro-holmquistite (Fhlm) in a dyke (a), platy-crystal sample (b), and acicular-crystal sample (c). Even in acicular-crystal samples, a small amount of platy crystals is present.

Ferro-holmquistite occurs as platy or acicular crystals. The platy crystals reach up to approximately 1 cm in length and about 2 mm in width and show dark blue color with a vitreous luster (Fig. 1b). These are commonly ac-

companied by white acicular crystals with widths of several micrometers and often occur in an asbestos-like habit (Fig. 1c); however, from one specimen, a bundled aggregate composed solely of platy crystals without associated acicular crystals was obtained (Fig. 1b).

Ferro-holmquistite is biaxial (-) with the refractive indexes of $\alpha = 1.647(2)$, $\beta = 1.659(2)$, $\gamma = 1.665(2)$ under white light, with $2V_{calc.} = 70.1°$. Pleochroism is strong and varies from colorless to deep blue. Using the empirical formula and observed and normalized wt%, the Gladstone-Dale suitability values (Mandarino, 1981) were found to range from 0.027 to 0.053 (excellent-good).

RAMAN SPECTROSCOPY

Raman spectroscopy was conducted with a Renishaw inVia Reflex spectrometer using the green diode laser with $\lambda = 532$ nm at the Institute for Solid State Physics (ISSP), the University of Tokyo. The laser power was approximately 10 mW. Figure 2 shows the spectrum in the ranges 3400-3800 cm^{-1} for the platy-crystal sample.

Based on the OH-stretching bands in orthorhombic *Pnma* amphiboles such as holmquistite series, the four main bands, labeled A, B, C, and D, are assigned to local configurations as *M*1*M*1*M*3-O3H-(□, Na): *M*1*M*1*M*3 = MgMgMg, MgMgFe, MgFeFe, and FeFeFe for A, B, C, and D, respectively (e.g., Ishida and Hawthorne, 2003). Following Ishida and Hawthorne (2003), the four bands, A, B, C, and D, in holmquistite are located at 3658-3662, 3643-3648, 3628-3629, and 3611-3614 cm^{-1}, respectively. Thus, the four Raman peaks observed at 3658, 3645, 3629, and 3613 cm^{-1} in present ferro-holmquistite are interpreted to correspond to the A, B, C, and D bands, respectively. In ferro-holmquistite, where the *M*1 and *M*3 sites are occupied by Fe^{2+}, the predominance of the D band is reasonable, and this feature is consistent with the results of FTIR spectroscopic analysis of ferro-ferri-holmquistite (Nagashima et al., 2022).

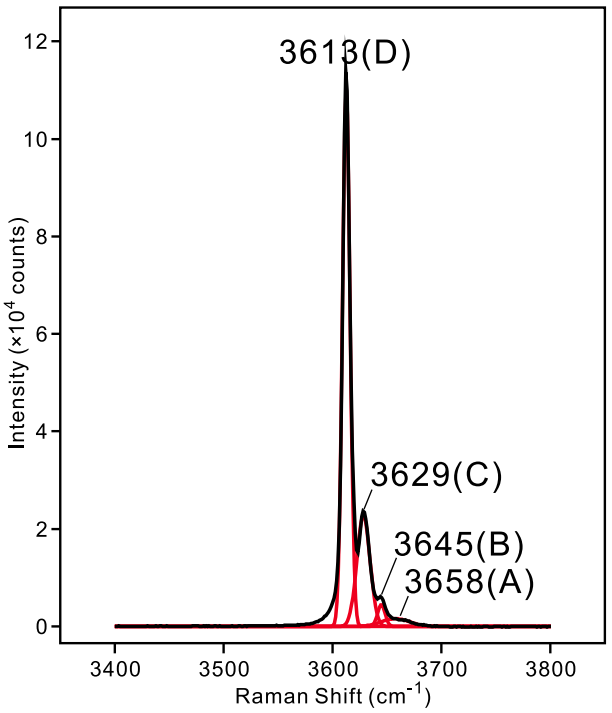

Figure 2. Raman spectrum of ferro-holmquistite. The black line is the observed spectrum after background subtraction, and the red line represents the Gaussian fitted peak. The letters in parentheses indicate local configurations (see text).

CHEMICAL COMPOSITION

Prior to electron microprobe analyses, the presence of Li was examined using inductively coupled plasma-atomic emission spectroscopy (ICP-AES; SPECTRO ARCOS, AMETEK) at ISSP. The platy-crystal sample were ground in an agate mortar, treated with a 1:1 mixture of nitric and hydrochloric acids, and then nebulized and introduced into an Ar plasma. The emitted light released during the relaxation of excited elements to their ground states was analyzed spectroscopically, and a strong emission line characteristic of Li was clearly observed at 670.78 nm (Supplementary Fig. S1; Figs. S1-S3 are available online from https://doi.org/10.2465/jmps.251128b). However, because the sample was not completely dissolved and residues remained, quantitative evaluation could not be performed.

Chemical analyses were carried out using a JEOL JXA-8230 electron microprobe (WDS mode, 15 kV, 20 nA, and 1 μm beam diameter) at Yamaguchi University. The ZAF method was used for data correction. Albite, periclase, corundum, wollastonite, manganosite, hematite, and fluorite were employed as standards for Na, Mg, Al, Si, Mn, Fe, and F respectively. Neither the aggregates of plate crystals nor the aggregates with acicular crystals showed any zoning (Fig. S2). Furthermore, the compositions of each were very homogeneous, but slightly different from each other (Table 1).

Based on the single-crystal X-ray diffraction (XRD) analysis, *M*1 and *M*3 sites are suggested to be predominantly occupied by Fe^{2+}, whereas the *M*2 site is occupied by Al. This site assignment is also supported by previous studies (Cámara and Oberti, 2005; Nagashima et al., 2022). Accordingly, the Fe^{2+}/Fe^{3+} ratio was estimated as follows. The chemical composition was normalized as Si = 8 apfu, and 2 − Al apfu was assumed to correspond to Fe^{3+}. The amount of Fe^{2+} was then calculated by subtracting Fe^{3+} from the total Fe content. Allocating all Na to the *A* site results in a nearly consistent result with the sin-

Table 1. Chemical compositions of ferro-holmquistite by WDS analysis

Platy-crystal sample wt% (n = 10)				Acicular-crystal sample wt% (n = 10)			
	Avg.	Min.	Max		Avg.	Min.	Max
SiO_2	55.02	54.35	55.63	SiO_2	54.98	54.00	55.39
Al_2O_3	10.19	9.77	10.56	Al_2O_3	9.63	9.39	10.01
FeO	23.64	22.97	24.12	FeO	24.25	23.31	24.84
MnO	1.43	1.21	1.62	MnO	1.66	1.47	1.85
MgO	1.06	0.96	1.13	MgO	0.98	0.92	1.02
Na_2O	0.25	0.15	0.35	Na_2O	0.29	0.21	0.35
F	0.09	0.00	0.18	F	0.13	0.05	0.25
Total	91.68			Total	91.91		
Fe_2O_3*	2.32			Fe_2O_3*	3.18		
FeO*	21.56			FeO*	21.38		
Li_2O*	3.37			Li_2O*	3.39		
H_2O*	2.02			H_2O*	2.00		
-O=F	0.04			-O=F	0.06		
Total	97.27			Total	97.56		
	apfu				apfu		
□	0.93			□	0.92		
Na	0.07			Na	0.08		
Σ =	1			Σ =	1		
Li	1.97			Li	1.98		
Mg	0.03			Mg	0.02		
Σ =	2			Σ =	2		
Fe^{2+}	2.62			Fe^{2+}	2.60		
Mn	0.18			Mn	0.20		
Mg	0.20			Mg	0.19		
Al	1.75			Al	1.65		
Fe^{3+}	0.25			Fe^{3+}	0.35		
Σ =	5			Σ =	5		
Si =	8			Si =	8		
O	22.05			O	22.05		
F	0.04			F	0.06		
OH	1.96			OH	1.94		
Σ =	2			Σ =	2		

*Calculated values normalized at Si = 8, 2-Al = Fe^{3+}, total Fe-Fe^{3+} = Fe^{2+}, 2-Mg = Li, F + OH = 2 (see text).

gle-crystal XRD results. The presence of Li was confirmed, and the single-crystal XRD analysis also indicates that Li nearly fully occupies the *M*4 site. Therefore, Li content was adjusted by considering Mg in the *M*4 site. During this estimation, all Mn is treated as Mn^{2+} and F + OH = 2 apfu as in previous studies (Cámara and Oberti, 2005; Nagashima et al., 2022). The back-calculated total

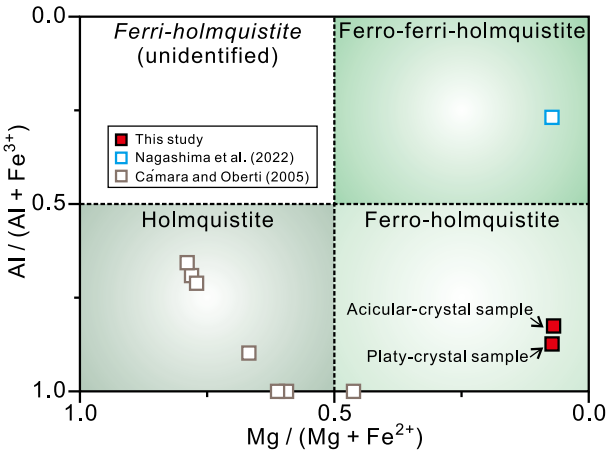

Figure 3. Comparison of chemical composition for holmquistite series.

wt% slightly below 100 may reflect the effects of beam damage. In contrast, EDS analyses performed under gentler beam conditions yield totals close to 100; however, WDS analysis is adapted to confirm the presence of F.

As a result, the empirical formulas are expressed as $(\square_{0.93}Na_{0.07})_{\Sigma1}(Li_{1.97}Mg_{0.03})_{\Sigma2}(Fe^{2+}_{2.62}Mg_{0.20}Mn_{0.18}Al_{1.75}Fe^{3+}_{0.25})_{\Sigma5}Si_8O_{22.05}(OH_{1.96}F_{0.04})_{\Sigma2}$ for the platy-crystal sample (Fig. 1b) and $(\square_{0.92}Na_{0.08})_{\Sigma1}(Li_{1.98}Mg_{0.02})_{\Sigma2}(Fe^{2+}_{2.60}Mn_{0.20}Mg_{0.19}Al_{1.65}Fe^{3+}_{0.35})_{\Sigma5}Si_8O_{22.05}(OH_{1.94}F_{0.06})_{\Sigma2}$ for the acicular-crystal sample (Fig. 1c). These compositions are close to the ideal formula and has a much higher Fe^{2+} content than the ferro-holmquistite reported by Cámara and Oberti (2005) (Fig. 3).

CRYSTALLOGRAPHY

Transmission electron microscopy

Amphiboles with vacancies at the *A* sites are known to crystallize in three structural types: proto, orthorhombic, and monoclinic structures. Among these, both the orthorhombic and monoclinic types have been reported in the holmquistite group. Therefore, it is essential to identify the structural type and corresponding proportion prior to single-crystal XRD analysis. Therefore, transmission electron microscopy (TEM) observations were conducted using a microscope (2100 TEM, JEOL) at ISSP operated at 200 kV because electron diffraction from the [010] direction provides high sensitivity to distinguish between these types. The results revealed that the ferro-holmquistite examined in this work is purely of the orthorhombic type (Fig. 4).

Powder X-ray diffraction

The powder XRD patterns were collected at room temper-

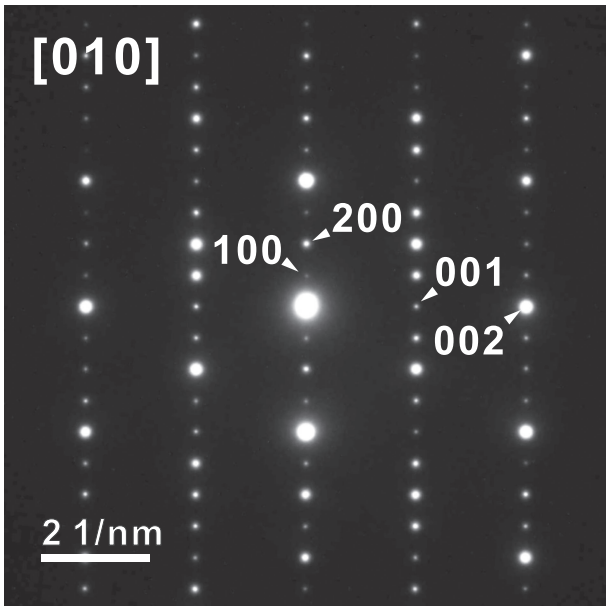

Figure 4. Selected-area electron diffraction pattern from [010] direction of ferro-holmquistite. The 100 and 001 reflections are visible due to multiple diffractions.

ature using a SmartLab diffractometer (Rigaku) with Cu*K*α radiation at ISSP. Because platy-crystal sample (Fig. 1b) is scarce, the acicular-crystal sample (Fig. 1c), which is more abundant, was used for this aim. The lattice parameters refined by least-squares fitting using 31 peaks with a large *d*-value were a = 18.407(7) Å, b = 17.767(6) Å, c = 5.298(2) Å, and V = 1732.6(11) Å^3 in the orthorhombic space group *Pnma* (#62) (Supplementary Table S1; Table S1 is available online from https://doi.org/10.2465/jmps.251128b). The parameters [d in Å ($I_{obs.}$) *hkl*] for the seven observed strongest lines of the powder XRD pattern were 8.156 (69) 210, 4.442 (8) 040, 3.196 (6) 440, 3.018 (100) 610, 2.810 (6) 251, 2.721 (13) 630, and 2.659 (6) 351, while it should be noted that the observed intensities differ from the ideal intensities due to the strong preferred orientation.

Single-crystal X-ray diffraction

The single-crystal XRD data was collected using a diffractometer (XtaLAB Synergy-R/DW, Rigaku) with Mo*K*α radiation and equipped with VariMax DW optics and an HyPix6000HE detector (Rigaku) at Yamaguchi University. The crystal of platy-crystal sample (Fig. 1b) was mounted on a glass fiber, and intensity data were measured at room temperature. The diffraction data and empirical absorption correction were processed using CrysAlisPro (Agilent, 2014). The SHELXL-2019/2 software (Sheldrick, 2015) was used for refinement of the crystal structure with neutral atom-scattering factors. The structure was solved by a direct method, and the resulting structure was found to be identical to that previously reported. Therefore, the site nomenclature follows that of the previous study (Hawthorne and Oberti, 2007). The H position was estimated from difference Fourier analysis, and the displacement parameter for the H atom was fixed at U_{iso} = 0.05 Å^2 with application of a restraint of O-H = 0.980(1) Å (Franks, 1973).

Ferro-holmquistite contains Fe and Mn with similar X-ray scattering factors. However, since Mn is trace amounts (Table 1), the refinements were performed as Fe. The occupancies were examined for Mg and Fe at the *M*1 and *M*3 sites, and for Al and Fe at the *M*2 sites. The *M*4 site is characterized by a 5+1 coordination environment, which is considered unfavorable for Na but favorable for Mg (Cámara and Oberti, 2005). Thus, Li and Mg were examined as candidate cations for the *M*4 site. In contrast, the *A* site was initially treated as vacant during structure refinement, yielding an R_1 value of 1.71%. However, inspection of the difference Fourier map revealed peaks at two symmetrically related atomic positions (Fig. S3). The midpoint between these two peaks corresponds to the conventional *A* site; however, this residual could not be resolved by examining the temperature factor after placing Na at this position. Subsequently, Na was placed at the two peak positions identified in the difference Fourier map, and refinement was carried out. In this model, both the atomic coordinates and site occupancies were successfully refined, leading to an improved R_1 value of 1.59%.

Details of the sample, data collection, and structure refinement are provided in Table 2 and the CIF, the FCF, and the RES files (Supplementary files are available online from https://doi.org/10.2465/jmps.251128b). The final atom coordinates, refined site occupancies, and thermal displacement parameters are summarized in Table 3. Selected interatomic distances are shown in Table 4. Table 5 lists the bond valences, which were calculated using the bond-valence parameters of Gagné and Hawthorne (2015). Both the bond-valence calculation and located hydrogen sites indicated that the O3A and O3B sites host OH groups. On the other hand, it is noted that because of the low Na occupancy, the bond-valence contributions associated with the *A* site were calculated to be negligible (zero) and are thus omitted from Table 5. The refined unit-cell parameters were a = 18.4080(3) Å, b = 17.7942(3) Å, c = 5.29463(11) Å, V = 1734.29(6) Å^3.

The refined crystal structure of ferro-holmquistite drawn by VESTA 3 (Momma and Izumi, 2011) is shown in Figure 5. This is a three-dimensional structure in the orthorhombic *Pnma* space group that consists of octahedrally coordinated *M*1-3 sites, 5+1 coordinated *M*4 sites, and tetrahedral double chains.

Table 2. Experimental details for single-crystal XRD analysis of ferro-holmquistite

Crystal size (mm)		0.32 × 0.18 × 0.08
Space group		*Pnma*
Unit-cell dimensions	*a* (Å)	18.4080(3)
	b (Å)	17.7942(3)
	c (Å)	5.29463(11)
	V (Å^3)	1734.29(6)
$D_{calc.}$ (g/cm^3)		3.23
Radiation		Mo*K*α (λ = 0.71073 Å)
Monochromator		VariMax optics
Diffractometer		Rigaku XtaLAB Synergy-R/DW with HyPix-6000HE
Scan type		ω scan
Absorption correction		CrysAlis^{Pro} (Agilent, 2014)
Absorption coefficient μ (mm^{-1})		3.17
θ_{min}-θ_{max} (°)		2.2-37.8
Collected reflections		31544
Unique reflctions ($I > 2\sigma$)		4199
R_{int} (%)		1.34
Index ranges	*h*	−31 → 29
	k	−25 → 30
	l	−5 → 9
Refinement on F^2 using		SHELXL-2019/2 (Sheldrick, 2015)
R_1 (%)		1.59
wR_2 (%)		5.21
No. of parameters		200
Weighting scheme*		$w = 1/[\sigma^2(F_o^2) + (0.0271P)^2 + 0.5751P]$
$\Delta\rho_{max}$ (e Å^{-3})		0.44
$\Delta\rho_{min}$ (e Å^{-3})		−0.61

* The function of the weighting scheme is $w = 1/[\sigma^0(F_o^2) + (a \cdot P)^2 + b \cdot P]$, where $P = [\mathrm{Max}(F_o^2) + 2F_c^2]/3$, and the parameters *a* and *b* are chosen to minimize the differences in the variances for reflections in different ranges of intensity and diffraction angle.

DISCUSSION

The ferro-holmquistite sample is characterized by high Fe^{2+} and Al contents. The discovery of this particular composition enables a more detailed discussion of the structural effects of Fe^{2+} by comparison with the data reported by Cámara and Oberti (2005), and of Fe^{3+} through comparison with the ferro-ferri-holmquistite reported by Nagashima et al. (2022). In this study, the primary focus was the influence of Fe^{2+} on the *M* octahedra and tetrahedra. The effect of Fe^{3+} is also discussed in a similar context.

The *M*2-O distance is clearly shorter than the *M*1-O and *M*3-O distances (Table 4). Iron at the *M*2 site is assumed to be Fe^{3+}, while at the *M*1 and *M*3 sites is Fe^{2+}, as supported by the bond-valence sums for the octahedral sites (Table 5). Accordingly, the effect of Fe^{2+} at the *M*1 and *M*3 sites, and of Fe^{3+} at the *M*2 sites on the structural variation can be evaluated on the basis of the Fe occupancies. The Mn^{2+} content is very small compared with that of Fe^{2+} (0.17 apfu for Mn^{2+}; Table 1) and thus cannot be distinguished from Fe^{2+} based on the X-ray scattering factors. Therefore, the effect of Mn^{2+} is considered to be merged with that of Fe^{2+} and is regarded as negligible in the present discussion.

Effect of Fe^{2+}

Figure 6 shows variations related to the *M* octahedra. The Al/Fe^{3+} ratio for the ferro-holmquistite sample is within the range reported by Cámara and Oberti (2005); therefore, the effects of Fe^{2+} in the present ferro-holmquistite sample can be better discussed based on data from Cámara and Oberti (2005). It is noted that the characteristics of ferro-ferri-holmquistite (Nagashima et al., 2022) are affected by Fe^{3+} at the *M*2 sites; therefore, although the data are plotted, they will not be considered in this discussion.

First, Fe^{2+} is equally distributed between the *M*1 and *M*3 sites in the present ferro-holmquistite (Fig. 6a). On the other hand, when the Fe^{2+} content was intermediate, Fe^{2+} tended to be distributed more predominantly to the *M*1 site, similar tendency was also found in sodic amphibole (Oberti et al., 2007). In monoclinic amphiboles, it has been suggested that, for intermediate compositions, the distribution of Fe^{2+} between *M*1 and *M*3 is influenced by cation size in the *M*2 site (Hawthorne, 1983), and a similar effect may occur in orthorhombic amphiboles. Also, Cámara and Oberti (2005) proposed that Fe^{2+} increases the distortion without changing the octahedral volume. However, the present results show a clear increase in the *M*1 and *M*3 octahedral volumes as the Fe occupancy increases (Fig. 6b).

The distortion, as measured by the quadratic elongation, remained constant in the *M*1 octahedron (especially when Fe > 0.3), which implies almost isotropic expansion (Fig. 6c). In contrast, distortion of the *M*3 octahedron increased as the Fe occupancy increased (Fig. 6c). Specifically, the *M*3-O1A and *M*3-O1B bond lengths increased (Fig. 6d), while the O1A-O1B distance was slightly shortened (Fig. 6e), which suggests elongation mainly along the ***b***-axis rather than the ***a***-axis. An anisotropic axial response indicates a stronger correlation between Fe occupancy in the *M*3 site and the *a*/*b* ratio compared to that with Fe occupancy in the *M*2 site (Figs. 6f and 6g). This suggests that structural changes associated with an increase in Fe^{2+} are mainly initiated by deformation of the *M*3 octahedron, which is contrary to the conventional idea that the *M*2 octahedron controls the structure. On the other

Table 3. Refined atomic positions with occupancy and anisotropic displacement parameters (Å^2) for ferro-holmquistite

	W	*x*	*y*	*z*	U_{eq}	Occupancy
*A*1	4*c*	0.3294(8)	0.25	0.562(3)	0.033(4) (U_{iso})	$Na_{0.055(3)}$
*A*2	4*c*	−0.0839(10)	0.25	0.204(3)	0.043(5) (U_{iso})	$Na_{0.051(3)}$
*M*1	8*d*	0.12524(2)	0.15789(2)	0.39789(2)	0.00633(4)	$Fe_{0.8504(17)}Mg_{0.1496}$
*M*2	8*d*	0.12542(2)	0.06706(2)	−0.10063(3)	0.00492(5)	$Al_{0.8443(15)}Fe_{0.1557}$
*M*3	4*c*	0.12533(2)	0.25	−0.10262(3)	0.00594(5)	$Fe_{0.849(2)}Mg_{0.151}$
*M*4	8*d*	0.12349(8)	−0.00860(10)	0.4012(3)	0.0191(5)	$Li_{0.976(2)}Mg_{0.024}$
Si1A	8*d*	0.26872(2)	0.16203(2)	0.07030(4)	0.00535(4)	$Si_{1.0}$
Si1B	8*d*	−0.01819(2)	0.16237(2)	0.72689(4)	0.00542(4)	$Si_{1.0}$
Si2A	8*d*	0.27362(2)	0.07660(2)	0.57697(4)	0.00552(4)	$Si_{1.0}$
Si2B	8*d*	−0.02416(2)	0.07745(2)	0.21830(4)	0.00560(4)	$Si_{1.0}$
O1A	8*d*	0.18041(3)	0.15474(3)	0.04995(10)	0.00700(8)	$O_{1.0}$
O1B	8*d*	0.07002(3)	0.15429(3)	0.74528(10)	0.00717(8)	$O_{1.0}$
O2A	8*d*	0.18506(3)	0.07367(3)	0.59717(9)	0.00758(8)	$O_{1.0}$
O2B	8*d*	0.06451(3)	0.07309(3)	0.20036(10)	0.00750(8)	$O_{1.0}$
O3A	4*c*	0.18291(4)	0.25	0.55735(15)	0.00941(12)	$O_{1.0}$
O3B	4*c*	0.06799(4)	0.25	0.23855(15)	0.00940(12)	$O_{1.0}$
O4A	8*d*	0.31346(3)	−0.00277(3)	0.56929(10)	0.00923(8)	$O_{1.0}$
O4B	8*d*	−0.06544(3)	−0.00015(3)	0.26687(10)	0.00938(8)	$O_{1.0}$
O5A	8*d*	0.30496(3)	0.11706(3)	−0.16436(10)	0.00946(8)	$O_{1.0}$
O5B	8*d*	−0.05398(3)	0.11603(3)	0.95771(10)	0.00950(8)	$O_{1.0}$
O6A	8*d*	0.29612(3)	0.12896(3)	0.33699(10)	0.01020(9)	$O_{1.0}$
O6B	8*d*	−0.04596(3)	0.13199(3)	0.45631(10)	0.01055(9)	$O_{1.0}$
O7A	4*c*	0.29166(4)	0.25	0.05338(16)	0.01071(12)	$O_{1.0}$
O7B	4*c*	−0.04095(4)	0.25	0.75193(16)	0.01083(12)	$O_{1.0}$
H3A	4*c*	0.23607(10)	0.25	0.566(5)	0.05 (U_{iso})	$H_{1.0}$
H3B	4*c*	0.0153(2)	0.25	0.212(5)	0.05 (U_{iso})	$H_{1.0}$

	U^{11}	U^{22}	U^{33}	U^{12}	U^{13}	U^{23}
*M*1	0.00771(5)	0.00651(5)	0.00477(5)	0.00002(3)	0.00051(3)	0.00005(3)
*M*2	0.00502(8)	0.00491(8)	0.00481(8)	0.00000(5)	−0.00005(5)	0.00018(5)
*M*3	0.00742(7)	0.00458(7)	0.00583(7)	0	−0.00041(4)	0
*M*4	0.0193(7)	0.0247(8)	0.0133(7)	0.0042(5)	0.0041(5)	0.0019(5)
Si1A	0.00578(7)	0.00553(7)	0.00473(7)	0.00037(5)	0.00003(5)	0.00001(5)
Si1B	0.00582(7)	0.00537(7)	0.00507(7)	−0.00035(5)	0.00009(5)	−0.00015(5)
Si2A	0.00585(7)	0.00589(7)	0.00483(7)	0.00089(5)	−0.00008(5)	0.00006(5)
Si2B	0.00588(7)	0.00604(7)	0.00489(7)	−0.00076(5)	0.00023(5)	0.00012(5)
O1A	0.00546(17)	0.00808(19)	0.00745(19)	0.00026(14)	0.00012(14)	0.00021(14)
O1B	0.00540(17)	0.00837(18)	0.00774(19)	−0.00018(14)	0.00020(14)	−0.00029(14)
O2A	0.00566(17)	0.00907(19)	0.00802(19)	0.00024(14)	−0.00009(13)	0.00002(15)
O2B	0.00569(16)	0.00927(19)	0.00752(18)	−0.00010(14)	0.00036(14)	−0.00006(15)
O3A	0.0088(3)	0.0096(3)	0.0098(3)	0	0.0006(2)	0
O3B	0.0087(3)	0.0094(3)	0.0102(3)	0	0.0005(2)	0
O4A	0.01050(19)	0.00713(19)	0.0101(2)	0.00315(15)	0.00046(15)	−0.00038(15)
O4B	0.01035(19)	0.00801(19)	0.0098(2)	−0.00336(15)	−0.00012(15)	0.00137(15)
O5A	0.00769(17)	0.0136(2)	0.00708(19)	−0.00003(15)	0.00008(14)	−0.00427(16)
O5B	0.00749(18)	0.0134(2)	0.00764(19)	−0.00033(15)	0.00029(14)	0.00429(16)
O6A	0.00916(18)	0.0138(2)	0.00760(19)	−0.00089(16)	−0.00110(15)	0.00459(16)
O6B	0.00934(18)	0.0150(2)	0.00725(19)	0.00142(16)	−0.00082(15)	−0.00491(17)
O7A	0.0111(3)	0.0053(3)	0.0158(3)	0	0.0003(2)	0
O7B	0.0116(3)	0.0053(3)	0.0156(3)	0	0.0003(2)	0

Table 4. Selected bond lengths (Å), volumes (Å^3), and angles (°) for ferro-holmquistite

*M*1-	O1A	2.1044(5)	*M*4-	O2A	2.1224(18)	O1A-O1B	2.5945(8)
	O1B	2.1025(5)		O2B	2.1029(17)	Si1A-Si1A	3.1307(8)
	O2A	2.1381(5)		O4A	2.1157(15)	Si1B-Si1B	3.1186(8)
	O2B	2.1495(5)		O4B	2.0628(15)		
	O3A	2.1275(5)		O5A	2.3622(18)	Si1A-O7A-Si1A	149.17(6)
	O3B	2.1234(5)		O6B	2.7252(18)	Si1B-O7B-Si1B	148.52(6)
	<*M*1-O>	2.1242		<*M*4-O>	2.2485	O5A-O6A-O5A	168.48(4)
	Volume	12.3913				O5B-O6B-O5B	166.21(4)
	Q.E.*	1.0209	Si1A-	O1A	1.6342(5)		
				O5A	1.6214(5)		
				O6A	1.6107(5)		
*M*2-	O1A	2.0235(5)		O7A	1.6239(3)		
	O1B	2.0285(5)		<Si1A-O>	1.6226		
	O2A	1.9441(5)					
	O2B	1.9515(5)	Si2A-	O2A	1.6344(5)		
	O4A	1.8396(5)		O4A	1.5920(5)		
	O4B	1.8471(5)		O5A	1.6514(5)		
	<*M*2-O>	1.9391		O6A	1.6291(5)		
	Volume	9.5958		<Si2A-O>	1.6267		
	Q.E.*	1.0101					
			Si1B-	O1B	1.6329(5)		
*M*3-	O1A×2	2.1340(5)		O5B	1.6148(5)		
	O1B×2	2.1415(5)		O6B	1.6143(5)		
	O3A	2.0892(8)		O7B	1.6200(3)		
	O3B	2.0921(8)		<Si1B-O>	1.6205		
	<*M*3-O>	2.1221					
	Volume	12.1672	Si2B-	O2B	1.6367(5)		
	Q.E.*	1.0313		O4B	1.5970(5)		
				O5B	1.6360(5)		
				O6B	1.6403(5)		
				<Si2B-O>	1.6275		

* Quadratic elongation (Q.E.) defined by Robinson et al. (1971).

Table 5. Bond-valence analysis results for ferro-holmquistite weighted by the refined site occupancies*

	*M*1	*M*2	*M*3	*M*4	Si1A	Si1B	Si2A	Si2B	Sum
O1A	0.36	0.38	0.34×2↓		0.97				2.05
O1B	0.36	0.38	0.33×2↓			0.98			2.05
O2A	0.34	0.47		0.19			0.97		1.97
O2B	0.33	0.46		0.20				0.97	1.96
O3A	0.34×2→		0.37						1.05
O3B	0.35×2→		0.37						1.07
O4A		0.62		0.20			1.09		1.91
O4B		0.61		0.21				1.07	1.89
O5A				0.13	1.01		0.93		2.07
O5B						1.02		0.97	1.99
O6A					1.03		0.99		2.02
O6B				0.08		1.03		0.96	2.07
O7A					1.00×2→				2.00
O7B						1.01×2→			2.02
Sum	2.08	2.92	2.08	1.01	4.01	4.04	3.98	3.97	

* The *A* sites excluded from this table because its contribution was negligible due to its very low Na concentration. In the case that the identical bonds bind to the same cation/anion, the number with the arrow (→ for anion and ↓ for cation) was added.

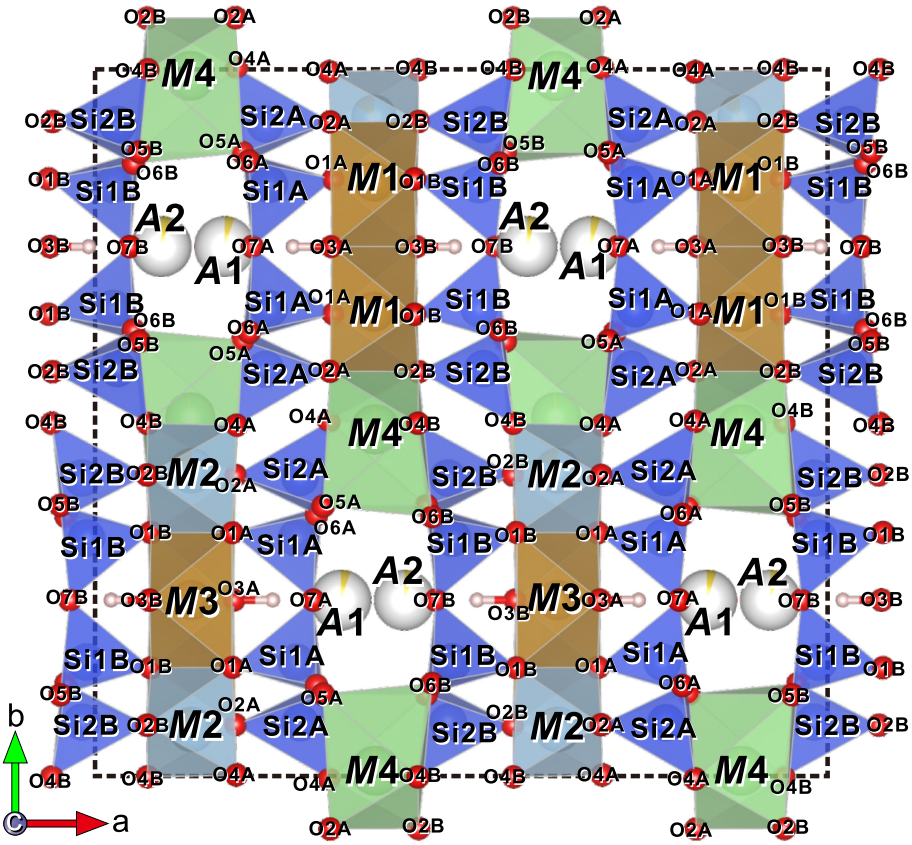

Figure 5. Crystal structure of ferro-holmquistite projected along [001] direction.

hand, the influence of octahedral distortion on the ***c***-axis direction remains minor. The *M*3 octahedral distortion may also relieve strain in the *M*2 octahedron because its quadratic elongation is lower than that in the data of Cámara and Oberti (2005) (Fig. 6h).

To accommodate these changes, the tetrahedra respond by chain kinking and/or adjustment of their volume via changes in the Si-O bond strength. The Si1-O7-Si1 angle tracks ***b***-axis stretching, and the O5-O6-O5 angle reflects ***c***-axis stretching. Figure 7a shows that an increase in Fe occupancy at the *M*3 site results in increased chain extension along the ***b***-axis, while changes along the ***c***-axis remain minimal (Fig. 7b). The Si1-Si1 distances via O7 along the ***b***-axis direction increase with increasing Fe occupancy (Fig. 7c), which indicates expansion of the tetrahedral volume. Structural changes induced by an increase in Fe occupancy at the *M*3 site may ultimately affect O7. The O7 atom is shared by two Si tetrahedra and the *A* site; however, because the *A* site is effectively vacant, the influence of tetrahedral change is expected to be accommodated primarily by O7. To evaluate this effect, we focused on the bond-valence sum of O7. As the Fe occupancy at the *M*3 site increases, the bond-valence sum of O7 was observed to approach the ideal value of 2.0 (Fig. 7d, Table 5).

In conclusion, Fe^{2+} can dominate over Mg at the *M*1 and *M*3 sites, where it is evenly distributed. The incorporation of Fe^{2+} increases the octahedral volume and induces anisotropic distortion, especially at *M*3 along the ***b***-axis. The *M*2 octahedra may also be indirectly affected by Fe^{2+} through interactions with neighboring octahedra. To accommodate these changes, the tetrahedral framework adjusts accordingly, which improves the bond-valence environment around the O7 site.

Effect of Fe^{3+}

The ferro-holmquistite and ferro-ferri-holmquistite samples reported by Nagashima et al. (2022) have almost identical Fe occupancies at the *M*1 and *M*3 sites (Fig. 6a); therefore, the structural differences between these two compositions can primarily be interpreted as reflecting the effect of increased Fe occupancy at the *M*2 sites. In this section, we compare the ferro-holmquistite and ferro-ferri-holmquistite samples. For reference, the data from Cámara and Oberti (2005) are also plotted in the figures.

It is clear that an increase in Fe occupancy leads to an increase in the volume of the *M*2 octahedron (Fig. 8a), as well as the ***a***- and ***b***-axes (Fig. 8b). This increase in Fe occupancy may also slightly increase the volume of the

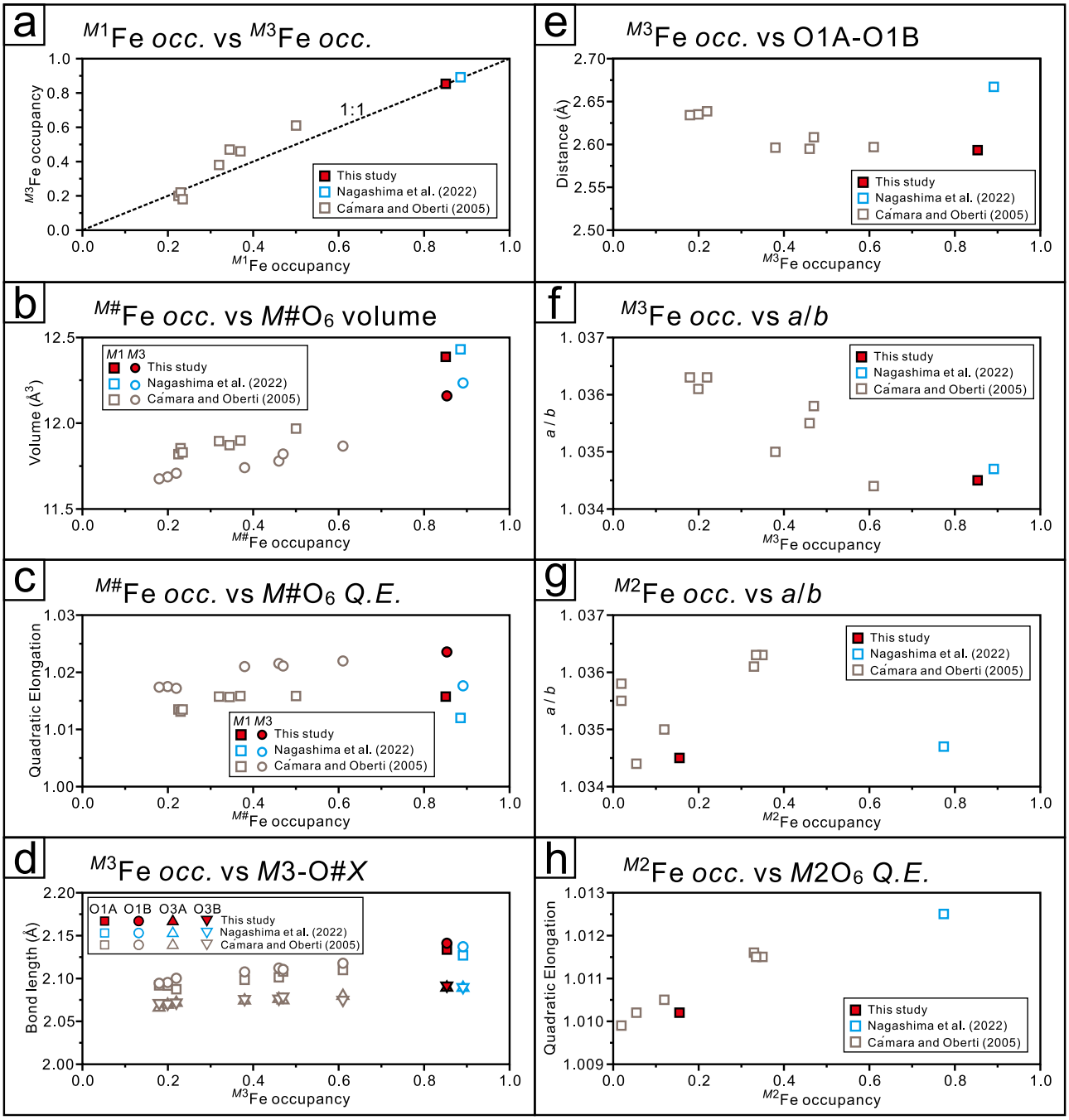

Figure 6. Vriations with respect to Fe occupancies in the *M* sites.

*M*1 and *M*3 octahedra (Fig. 6b). The effect of the reduction in the distortion of the *M*1 and *M*3 octahedra is, however, clear (Fig. 6c). The *M*2 octahedron becomes significantly distorted with increasing Fe^{3+} content (Fig. 6h). As a result, the *a*/*b* ratio only increases slightly, even with a large increase in Fe^{3+} content (Figs. 6f and 6g).

The structural adjustment of the tetrahedron associated with the increase in Fe^{3+} content would induce bending of the chain along the ***b***-axis (Fig. 7a) and elongation along the ***c***-axis (Fig. 7b). This would result in a significant decrease in the Si1–Si1 distance (Fig. 7c) and also cause the bond valence sum at O7A to deviate from the ideal value (Fig. 7d).

Taken together, within the compositional range between ferro-holmquistite and ferro-ferri-holmquistite, these observations suggest that the amount of Fe^{3+} in the *M*2 octahedron influences the behavior of the other octahedra and tetrahedra. However, it should be noted that this

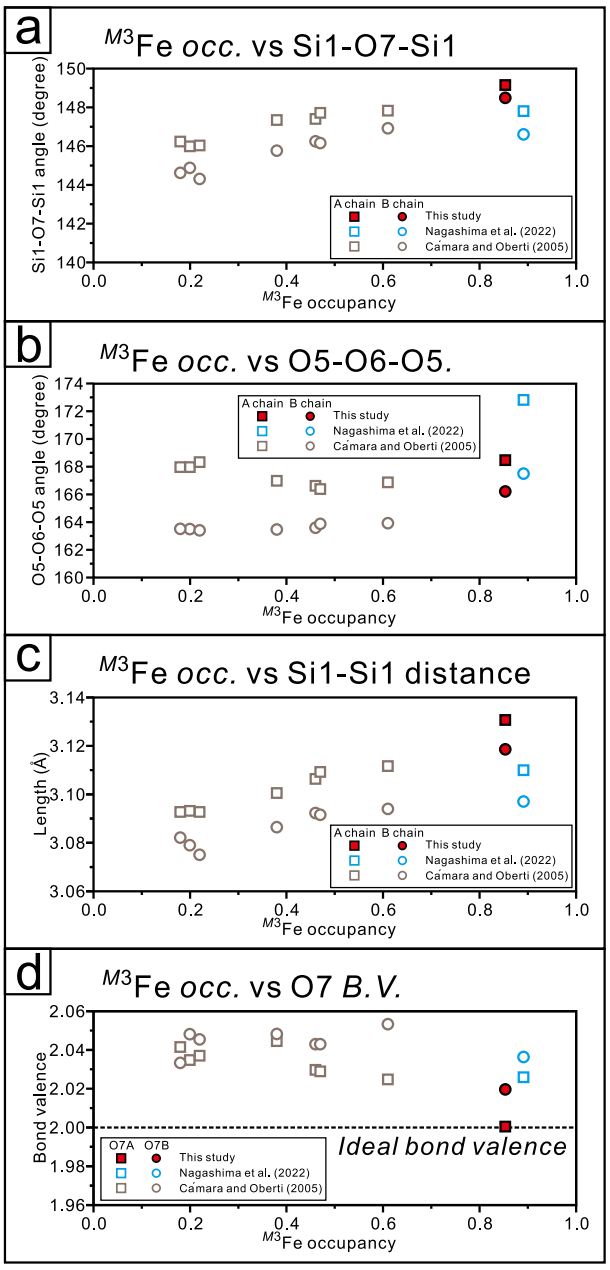

Figure 7. Changes in silicate chain with respect to Fe occupancy at *M*3 site.

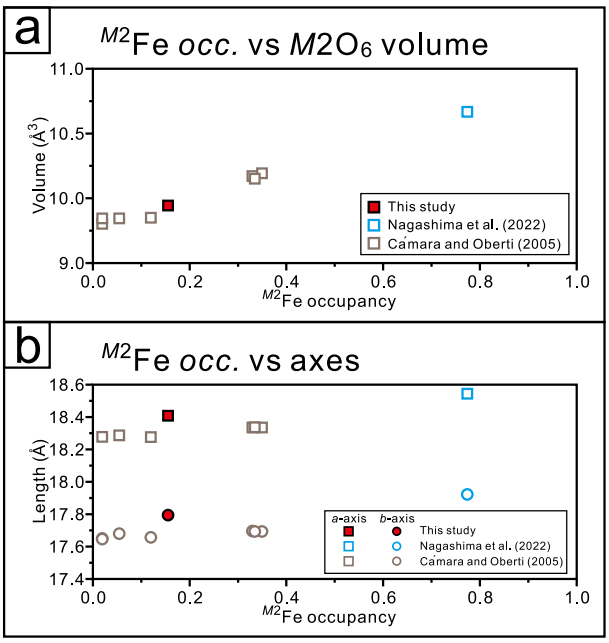

Figure 8. Variations in $M2O_6$ volume and lengths of ***a***- and ***b***-axes as function of Fe occupancy at *M*2 site.

does not support previous claims that the *M*2 octahedron controls the amount of Fe^{2+} in the other octahedra, because the ferro-holmquistite and ferro-ferri-holmquistite samples reported by Nagashima et al. (2022) have almost identical Fe occupancies at the *M*1 and *M*3 sites (Fig. 6a). The important aspect is that the overall structure is capable of accommodating Fe^{2+} and/or Fe^{3+}.

Geometrical constraints

Cámara and Oberti (2005) predicted that the presence of a small monovalent cation such as Li at the *M*4 site would impose geometrical constraints on the crystal structure. They proposed that this would induce underbonding at the O4A and O4B sites, which would constrain the *M*2–O4 distance to be shorter. This would result in a distortion of the *M*2 octahedron along the ***b***-axis, which would exert pressure on the *M*3 octahedron, and ultimately limit the occupancy of Fe^{2+} at the *M*3 site.

Nevertheless, both ferro-ferri-holmquistite and the present Fe^{2+}-rich ferro-holmquistite actually occur, and their Li content and degree of underbonding (bond valence sum: ~ 1.90) at the O4A and O4B sites are comparable to those reported by Cámara and Oberti (2005). Therefore, underbonding at the O4A and O4B sites is not associated with an increase in Fe^{2+} and/or Fe^{3+} content. This suggests that even if a small cation at the *M*4 site causes underbonding of O4A and O4B, it does not restrict the accommodation of Fe^{2+} and/or Fe^{3+} in any octahedron. The overall structure instead remains flexible to accommodate Fe^{2+} and/or Fe^{3+}, and currently, no definitive geometrical constraints can be predicted in the holmquistite structure.

CONCLUSION

In this study, ferro-holmquistite with a high Fe^{2+} content was discovered, which allowed the effects of Fe^{2+} and Fe^{3+} on the structure to be examined by comparison with previous studies. Fe^{2+} mainly expands the *M*1 and *M*3 octahedra, where notable anisotropic elongation and increased

strain in the ***b***-axis direction of the *M*3 octahedron are particularly prominent. On the other hand, an increase in Fe^{3+} increases the volume and distortion of the *M*2 octahedron, which suppresses the *M*1 and *M*3 octahedra. In response to these changes, the tetrahedra can modify their structural configurations through connection bending and volume change. The presence of a small cation at the *M*4 site contributes to underbonding of O4A and O4B; however, it does not impose any structural constraints that limit the incorporation of Fe^{2+} and/or Fe^{3+}.

ACKNOWLEDGMENTS

This study uses research equipment shared in the MEXT Project for Promoting Public Utilization of Advanced Research Infrastructure (Program for supporting construction of core facilities), grant No. JPMXS0440400024.

SUPPLEMENTARY MATERIALS

Supplementary Figures S1–S3, Table S1, CIF, FCF, and RES files are available online from https://doi.org/10.2465/jmps.251128b.

REFERENCES

Agilent (2014) CrysAlis PRO. Agilent Technologies Ltd, Yarnton, Oxfordshire, England.

Cámara, F. and Oberti, R. (2005) The crystal-chemistry of holmquistites: Ferroholmquistite from Greenbushes (Western Australia) and hints for compositional constraints in ^{B}Li amphiboles. American Mineralogist, 90, 1167–1176.

Ehiro, M., Kanisawa, S. and Taketani, Y. (1989) Pre-Tertiary Takine Group in the central Abukuma Massif. Bulletin of the Fukushima Museum, 3, 21–37 (in Japanese with English abstract).

Franks, F., Ed. (1973) Water: A comprehensive treatise, vol. 2, pp. 684, Plenum, New York.

Gagné, O.C. and Hawthorne, F.C. (2015) Comprehensive derivation of bond-valence parameters for ion pairs involving oxygen. Acta Crystallographica, B71, 562–578.

Hawthorne, F. (1983) The crystal-chemistry of the amphiboles. The Canadian Mineralogist, 21, 173–480.

Hawthorne, F. and Oberti, R. (2007) Amphiboles: crystal chemistry. Reviews in Mineralogy and Gechemistry, 67, 1–54.

Ishida, K. and Hawthorne, F.C. (2003) Fine structure in the infrared OH-stretching bands of holmquistite and anthophyllite. Physics and Chemistry of Minerals, 30, 330–336.

Kubo, K., Yanagisawa, Y., Yamamoto, T., Komazawa, M., et al. (2003) Geological map of Japan 1:200,000, Fukushima. Geological Survey of Japan, AIST, NJ-54-16 22 (in Japanese with English abstract).

Mandarino, J.A. (1981) The Gladstone-Dale relationship: part IV. the compatibility concept and its application. The Canadian Mineralogist, 19, 441–450.

Momma, K. and Izumi, F. (2011) VESTA3 for three-dimensional visualization of crystal, volumetric and morphology data. Journal of Applied Crystallography, 44, 1272–1276.

Nagashima, M., Imaoka, T., Kano, T., Kimura, J., et al. (2022) Ferro-ferri-holmquistite, $\square Li_2(Fe^{2+}_3Fe^{3+}_2)Si_8O_{22}(OH)_2$, $Fe^{2+}Fe^{3+}$ analogue of holmquistite, from the Iwagi islet, Ehime, Japan. European Journal of Mineralogy, 34, 425–438.

Oberti, R., Hawthorne, F., Cannillo, E. and Cámara, F. (2007) Long-range order in amphibole. Reviews in Mineralogy and Geochemistry, 67, 125–171.

Omori, K. and Hasegawa, S. (1957) Minerals containing rare elements from the Hayamadake pegmatite in Tokiwa town, Fukushima Prefecture. The Journal of the Japanese Association of Mineralogists, Petrologists and Economic Geologists, 41, 1–9 (in Japanese with English abstract).

Robinson, K., Gibbs, G.V. and Ribbe, P.H. (1971) Quadratic elongation: a quantitative measure of distortion in coordination polyhedral. Science, 172, 567–570.

Sheldrick, G.M. (2015) Crystal structure refinement with SHELXL. Acta Crystallographica, C71, 3–8.

Manuscript received November 28, 2025
Manuscript accepted April 3, 2026
Advance online publication April 14, 2026
Released online publication May 8, 2026
Manuscript handled by Hiroki Okudera